Resonance based Current-fed Isolated DC/ DC Converter for High Voltage Applications

Vishal Anand A G
Member, IEEE
Bloom Energy (I) Pvt Ltd
Bangalore, India
vanand@bloomenergy.com

Kaushik Basu
Member, IEEE
Indian Institute of Science
Bangalore, India
basu@ee.iisc.ac.in

Ranganathan Gurunathan
Member, IEEE
Bloom Energy (I) Pvt Ltd
Bangalore, India
rgurunat@bloomenergy.com

***Abstract*—This paper presents a novel resonance based modulation strategy for a full-bridge current-fed isolated DC/ DC converter for high voltage applications. Output regulation is obtained using variable frequency modulation on the primary side to compensate for line and load variations. A two-step method is used for current commutation and usage of active clamp based snubbers are avoided. Circuit operation under different operating modes in steady state are described in detail. Closed form expression for the converter gain and other values of interest are derived using state plane concepts. The presence of a discontinuous conduction mode is discussed and the mode boundary is identified. Design steps for arriving at the component values of the converter based on set of specifications is discussed. Proposed concept, operation and derived closed form expressions are validated through simulation.**

I. Introduction

One of the major area in which isolated current-fed DC/ DC converters are used is high voltage industrial applications like medical X-ray imaging, radio frequency generation, lasers etc. [1]. This type of converter is suited for these application due to the absence of an output inductor and because they do not have flux imbalance problem of the isolation **H**igh **F**requency **T**ransformer (HFT) [2]. Current-fed converters have been demonstrated to be the topology of choice for power generation from **D**istributed **E**nergy **R**esources (DER) like solar photovoltaics, fuel cells etc. [3]. Another area of application of current-fed topologies is integration of DERs into DC microgrids [4]. HFTs are used to achieve the dual benefit of providing galvanic isolation and required converter turns ratio [5]. Among the different topologies proposed for these converters, the full bridge version is most suitable for the power levels upto a few kWs. **P**ulse **W**idth **M**odulation (PWM) on the primary bridge results in hard switching and voltage spikes during the switching transitions require special clamping circuits for operation [6]. Phase shifting on the primary with **D**ual **A**ctive **B**ridge (DAB) topologies have been proposed to address these issues [7]. Quasi-resonant based variable switching frequency modulation strategies are proposed in [2], [8]. This paper presents a full-bridge current-fed DC/ DC converter topology that employs a new resonant tank configuration. A resonant based novel control strategy is proposed. The exact analysis without the **F**irst **H**armonic **A**pproximation (FHA) is done along-with determination of the boundary between **C**ontinuous **C**onduction **M**ode (CCM) and **D**iscontinuous **C**onduction **M**ode (DCM). Design steps for selection of the resonant component is discussed. Simulations results are presented to validate the concept.

978-1-5386-9316-2/18/$31.00 © 2018 IEEE

II. Steady State Analysis

This section presents the steady state analysis of the converter. The analysis is divided into the following sub-sections (a) Circuit operation (b) Converter gain and (c) Output characteristics and discontinuous conduction mode

A. Circuit Operation

The architecture of the proposed converter is shown in Fig 1. Before getting into the operation of the converter, the per-unitization base quantities used for the purpose of analysis are defined in Table I.

TABLE I: Per-unitisation base parameters

Description	Formula
Base current, I_b	I_s
Base impedance, R_b	$\sqrt{\frac{L_r}{C_r}}$
Base voltage, V_b	$I_b R_b$
Base frequency, f_o	$\frac{1}{2\pi\sqrt{L_r C_r}}$

The presented analysis is similar to the exact analysis of voltage-fed parallel resonant converter [9]. The current source is realized with a DC source in-line with an inductor, L_s as shown in Fig 1. Primary devices, Q_1 to Q_4 are switched in complimentary fashion to generate a square wave current, i_s exciting the $C_r - L_r$ resonant tank network as shown in Fig 2. A two-step modulation technique is utilized to ensure that the resonant capacitor, C_r is not shorted in the commutation process of the primary devices. As seen in Fig 2, the commutation of devices Q_1 to Q_4 is performed in a two-step method wherein the devices in a leg that's going to conduct the current are turned ON before the conducting devices are turned OFF.

The response of the $C_r - L_r$ resonant tank to the applied square wave current input, i_s is a function of the base or

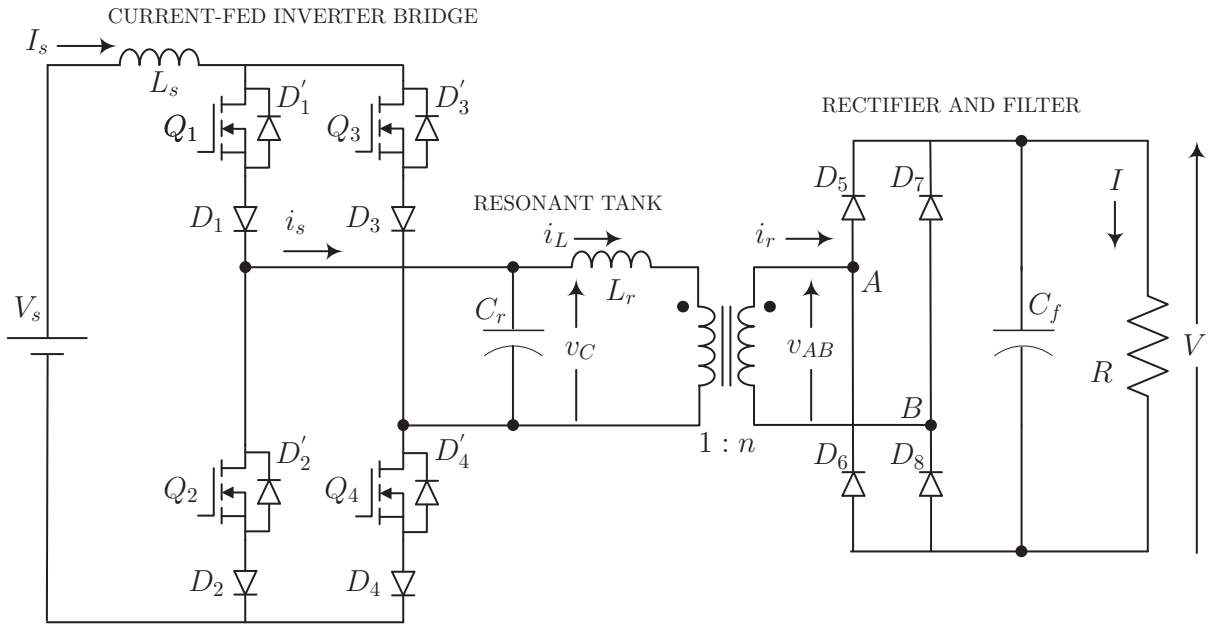

Fig. 1: Proposed topology for resonance based current-fed DC/ DC converter

resonant frequency, f_o and the switching frequency of the primary bridge, f_s. The secondary diode bridge, D_5 to D_8 rectifies the reflected inductor current, i_r. Average value of i_r flows into the load resistance, R and the output filter capacitance, C_f filters the high frequency component in the rectified current. The rectifier input voltage, v_{AB} can be modeled as a current dependent voltage source of magnitude V.

Table II describes the per-unitized circuit parameters that shall be used in the analysis of the current-fed resonant DC/ DC converter. In steady state operation, over one cycle of the switching current i_s, 4 operating modes of the circuit shall be observed based on the polarity of applied current, i_s and inductor current, i_L. Fig 3 plots the variation of key circuit parameters as a function of the normalized angle, θ. The zero state in the current excitation, i_s is not shown in this figure as this time period is negligible in comparison with the switching time. $m(0)$ and $j(0)$ are the initial conditions of the capacitor voltage, m_C and inductor current, j_L as shown here. As long as $j_L < 0$, the rectifier voltage, m remains at $-M$ because diodes D_6 and D_7 are in conduction. At the instant, $\theta = \alpha$, when $j_L = 0$, diodes D_5 and D_8 come into conduction and m changes to M from $-M$. Due to the presence of the diode bridge, the load characteristics can be modeled as a current dependent voltage source. At the instant, $\theta = \gamma$, the primary devices are switched as per the modulation explained in Fig 1 and i_s changes to -1 from $+1$. The remaining two modes

TABLE II: **P**er **U**nit (PU) converter parameters.

Description	Formula
Resonant capacitor voltage, m_C	$\frac{v_C}{V_b}$
Inductor current, j_L	$\frac{i_L}{I_b}$
Switching frequency, F	$\frac{f_s}{f_o}$
Rectifier current, j	$\frac{ni_r}{I_b}$
Rectifier voltage, m	$\frac{v_{AB}}{nV_b}$
Angular half-period, γ	$\frac{\pi}{F}$
Output voltage, M	$\frac{V}{nV_b}$
Converter gain, J	$\frac{I}{I_b}$

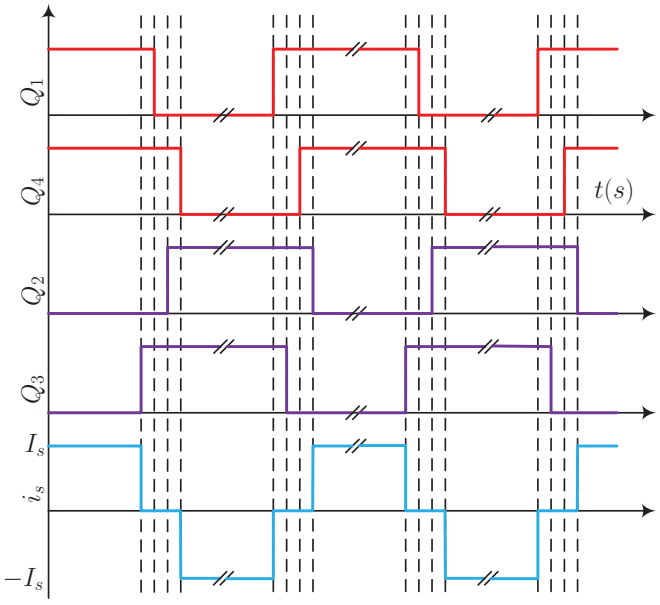

Fig. 2: Modulation of the primary devices in the current-fed resonant DC/ DC converter

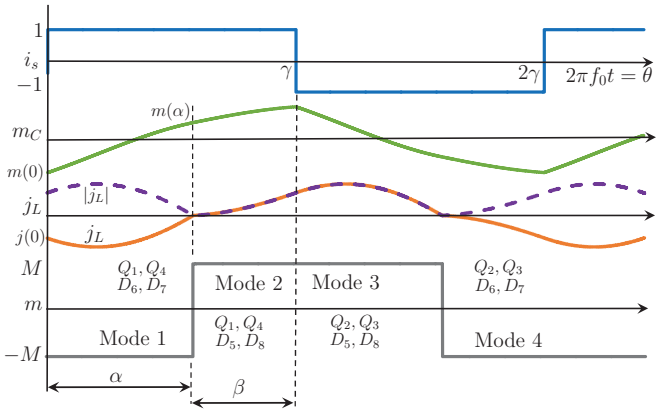

Fig. 3: Steady state waveforms of current-fed resonant DC/ DC converter over one switching cycle

of operation of the circuit are symmetrical to the previously described modes with a change in the initial conditions of the circuit. Analysis of these 4 modes is carried out by using the reduced equivalent circuit of the converter reflected on the primary side of the transformer as shown in Fig 4. The following sections describe the different equivalent circuits in each of the operating modes and the relevant state equations.

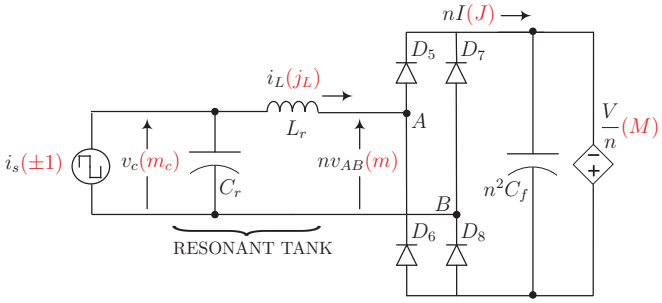

Fig. 4: Equivalent circuit of the current-fed resonant DC/ DC converter for analysis

1) Mode 1: As seen in Fig 3, the source current, i_s of magnitude $+1$ is applied to the resonant tank in this mode of operation. The per-unitized equivalent circuit during this mode of operation is shown in Fig 5.

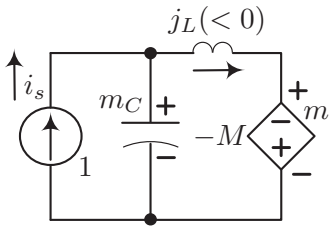

Fig. 5: Equivalent circuit of the current-fed resonant DC/ DC converter in Mode 1

The state equations of the converter in this mode of are given in Eq(1) and Eq(2).

$$\frac{dm_C}{d\theta} + j_L = 1 \tag{1}$$

$$\frac{dj_L}{d\theta} - M = m_C \tag{2}$$

2) Mode 2: As seen in Fig 3, the source current, i_s remains at magnitude $+1$ in this mode of operation. The resonant inductor current changes it's polarity to positive from negative. The per-unitized equivalent circuit during this mode is given in Fig 6.

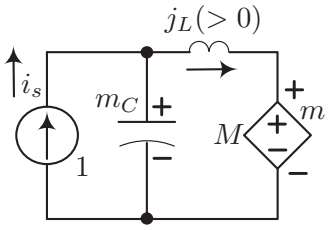

Fig. 6: Equivalent circuit of the current-fed resonant DC/ DC converter in Mode 2

The state equations of the converter in this mode are given in Eq(3) and Eq(4).

$$\frac{dm_C}{d\theta} + j_L = 1 \tag{3}$$

$$\frac{dj_L}{d\theta} + M = m_C \tag{4}$$

3) Mode 3: The source current, i_s changes it's polarity to -1 from $+1$ in this mode of operation as shown in Fig 3. The resonant inductor current remains positive during this mode. The per-unitised equivalent circuit during this mode of operation is given in Fig 7.

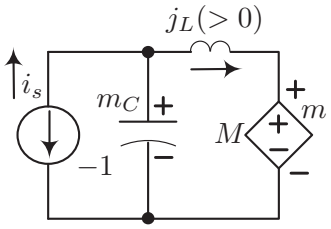

Fig. 7: Equivalent circuit of the current-fed resonant DC/ DC converter in Mode 3

The state equations of the converter in this mode are given in Eq(5) and Eq(6).

$$\frac{dm_C}{d\theta} + j_L = -1 \tag{5}$$

$$\frac{dj_L}{d\theta} + M = m_C \tag{6}$$

4) Mode 4: As seen in Fig 3, the source current, i_s remains at magnitude -1 in this mode of operation. The resonant inductor current changes it's polarity to negative from positive. The per-unitized equivalent circuit during this mode of operation is given in Fig 8. The state equations of the converter in this mode are given in Eq(7) and Eq(8).

$$\frac{dm_C}{d\theta} + j_L = -1 \tag{7}$$

$$\frac{dj_L}{d\theta} - M = m_C \tag{8}$$

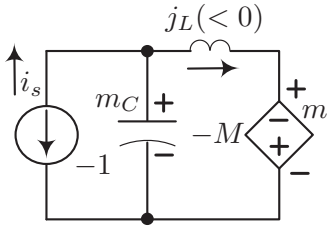

Fig. 8: Equivalent circuit of the current-fed resonant DC/ DC converter in Mode 4

B. Converter Gain

The variation between capacitor voltage, m_C and inductor current, j_L shown in Fig 3 can be plotted with respect to each other to get the state plane portrait of the converter. This is shown in Fig 9. The 4 operating modes described above are highlighted in Fig 9. As shown in Fig 4, average value of rectified inductor current, $|j_L|$ flows into the load. The converter gain is arrived at by getting a closed form expression for this current as given in Eq(9). The expression for $j(\theta)$ is written from Eq(3) and Eq(5). This is substituted in Eq(9) to arrive at Eq(10).

$$J = \frac{1}{\gamma}\int_{\alpha}^{\alpha+\gamma} j(\theta)d\theta \tag{9}$$

$$J = \frac{1}{\gamma}\Big\{\Big\{\int_{\alpha}^{\gamma} 1d\theta + \int_{\gamma}^{\gamma+\alpha} -1d\theta\Big\} - \Big\{\int_{\alpha}^{\gamma+\alpha} 1.dm_C\Big\}\Big\} \tag{10}$$

Eq(10) can be further simplified to arrive at the expression given below which equates the J with the angular half-period, γ which in-turn is a function of the operating frequency, F and the intermediate load dependent voltage, $m(\alpha)$ shown in Fig 3.

$$\frac{J\pi}{2F} = \phi + m(\alpha) \tag{11}$$

where,

$$\phi = \frac{\beta - \alpha}{2} \tag{12}$$

In order to arrive at the closed form solution for J, trigonometric identities are utilised to eliminate common terms. Fig 10 shows the positive portion of j_L which is averaged to arrive at J.

Equating the angles subtended as shown Fig 10 in with the initial condition $m(0)$ and using other identities, relationship in Eq(13) is arrived at. Similarly, initial conditions on $j(0)$ are equated and further simplifications results in the expression for $m(\alpha)$ given in Eq(14). Substituting $m(\alpha)$ from Eq(14) in Eq(11), we have the final expression for the converter gain of the current-fed resonant DC/ DC converter. The other parameters of interest, $m(0)$ and $j(0)$ can now be derived based on the existing relationships as given in Eq(16) and Eq(17). This completes the derivation on the important parameters that define the operation of the converter in the CCM mode.

$$m(\alpha)\cos\frac{\pi}{2F}\cos\phi = -\sin\phi\Big\{\cos\frac{\pi}{2F} + M\sin\frac{\pi}{2F}\Big\} \tag{13}$$

$$m(\alpha) = -\frac{\sin\phi}{\cos\frac{\pi}{2F}} \tag{14}$$

$$J = \frac{2F}{\pi}\Big\{\phi - \frac{\sin\phi}{\cos\frac{\pi}{2F}}\Big\} \tag{15}$$

$$j(0) = -M\frac{\sin\phi}{\cos\frac{\pi}{2F}} \tag{16}$$

$$m(0) = -(M^2-1)\tan\frac{\pi}{2F} \tag{17}$$

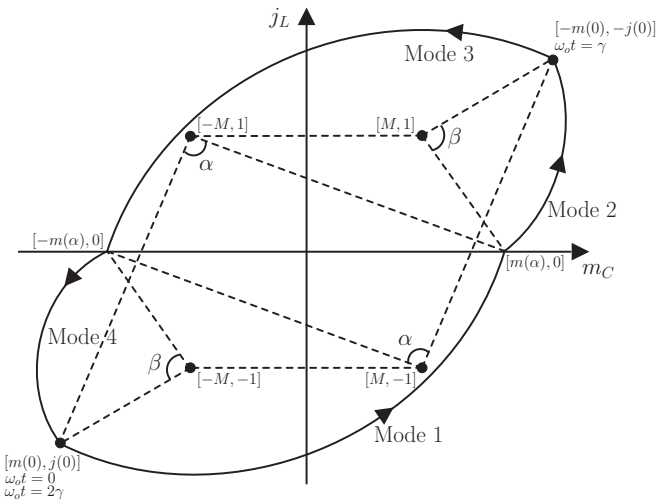

Fig. 9: State plane portrait of the current-fed resonant DC/ DC converter

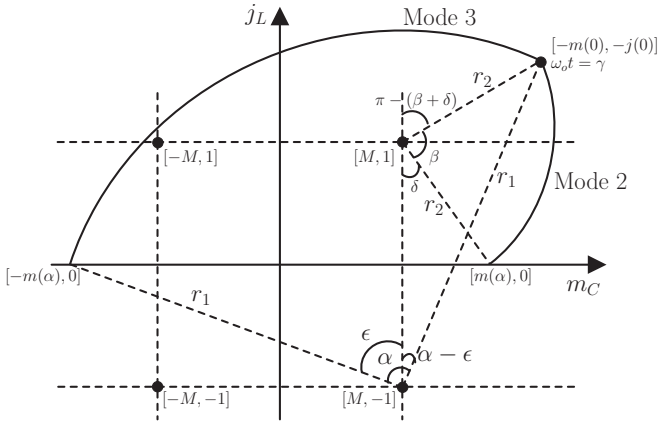

Fig. 10: Trigonometric identities applied on the state plane portrait to arrive at steady state converter gain

C. Output Characteristics and Discontinuous Conduction Mode

The output characteristics of the parallel resonant current-fed DC/ DC converter shall be plotted by varying the load for different operating frequencies and finding the current gain at each operating point as given in Eq(15). During the steady state operation of the converter, $m(\alpha)$ is the capacitor voltage at the boundary of mode 1 and mode 2. For diodes D_5 and D_8 to start conduction, $m(\alpha)$ must be greater than M. If under certain load condition $m(\alpha) < M$, these diodes shall be reverse biased and the output load shall be decoupled from the input. This introduces a DCM in the operation of the converter. The boundary of operation between the CCM and DCM modes in the output characteristice of the converter can be found by equating $m(\alpha)$ with M and solving for the applicable operating point, M_{crit} as given in Eq(18)

$$M_{crit} = -\frac{1}{2}\sin\frac{\pi}{F} + \sqrt{\sin^2\frac{\pi}{2F} + \frac{1}{4}\sin^2\frac{\pi}{F}} \tag{18}$$

The output characteristics of the current-fed resonant DC/ DC converter is shown in Fig 11. The "black" trace represents M_{crit} boundary between CCM and DCM for different values of switching frequency, F. The state plane portrait of the converter in the DCM mode of operation is shown in Fig 12. The discontinuous portion of the inductor current is highlighted during which there's a linear rise in the capacitor voltage along it's axis. There's no closed form expression for the converter gain in DCM mode of operation.

III. Design and Simulation Results

The following sections delve into the design steps of the converter to meet the required design specifications. Simulation results are provided to validate the topology.

A. Design Steps

The design is based on the specifications given in Table III. Design implies determination of the values of L_r, C_r and

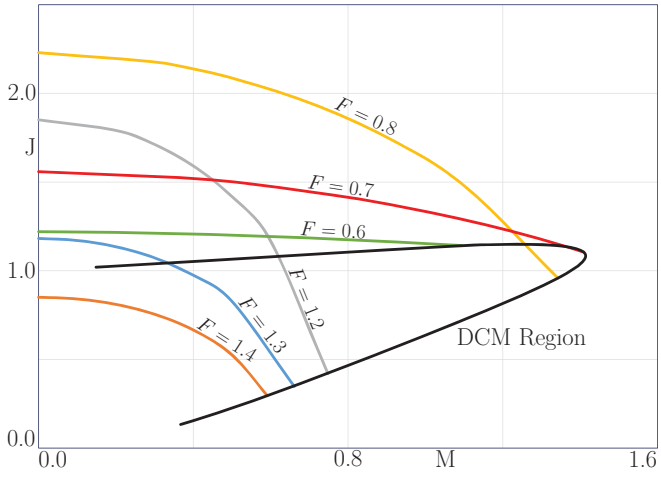

Fig. 11: Output characteristics of the current-fed resonant DC/ DC converter

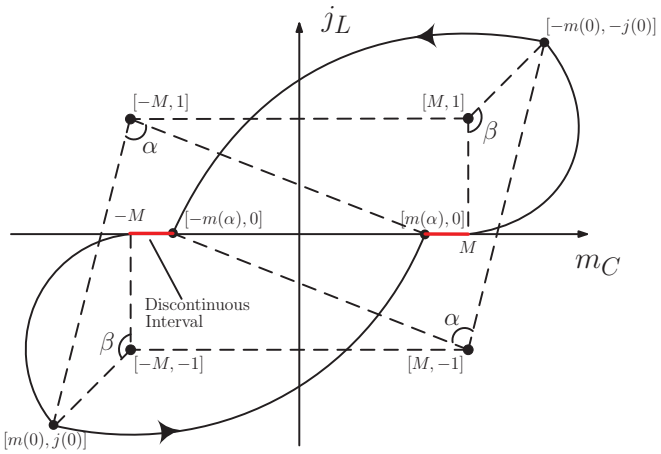

Fig. 12: State plane portrait of the current-fed resonant DC/ DC converter in DCM

turns ratio, n as shown in Fig 1. The first design choice made is in the selection of the resonant frequency, f_o. Since the proposed topology is derivative of the parallel resonant control structure, the behavior of the converter is valid in the range $0.5 < F < 2$ [9]. Based on this and from the design specification, $f_{s,max} = 100kHz$, the resonant frequency f_o will be $50kHz$.

TABLE III: Design specifications of current-fed DC/ DC

Description	Value
Input voltage, V_s	$48V$
Output voltage, V	$400V$
Output power, P_o	$1kW$
Max switching frequency, $f_{s,max}$	$100kHz$

In order to arrive at the design values of the resonant tank components, a design choice on maximum per-unit current gain, J_{max} and maximum load voltage, M_{max} is made by optimization on the device stresses, RMS currents and voltages in the resonant elements. Based on the chosen value of M_{max}, the transformer turns ratio is found from the specifications to be $n = \frac{N_s}{N_p} = \frac{103}{10}$. From J_{max} and M_{max} the value of base impedance, $R_b = 2.02\Omega$ is arrived. From R_b and resonant frequency, f_o tank inductance is calculated as $L_r = 6.4\mu H$ and tank capacitance, $C_r = 1.6\mu F$. This completes the design of current-fed DC/ DC converter.

B. Simulation Results

In order to validate the design, the rated operating point is chosen and the converter is simulated to validate the operation and the derived closed form expressions. Assuming negligible losses in the converter and from the specifications of input voltage, V_s and P_o we can arrive at the base current, $I_b = \frac{P_o}{V_s} = 20.83A$. The calculated load resistance at the rated operating condition is $R = \frac{V^2}{P_o} = 160\Omega$. From the known base quantities, I_b and R_b, V_b is found which in turn is used

to obtain the PU output voltage in the given operating point, $M = 0.75$. The load quality factor is, $Q = \frac{R}{n^2 R_{bp}} = 0.75$. Assuming negligible losses in the converter, we can apply power balance between input and output in Fig 1 and say that $V_s I_s = VI$. From this equality and the operating conditions provided, the current gain of the converter can be found to be $J = \frac{M}{Q} = 1.0$. From the values of M and J, the PU switching frequency of the converter, $F = 1.1$ is arrived at by solving Eq(15) recursively. This corresponds to a switching frequency of $f_s = F * f_o = 55kHz$. The converter is now simulated using LTSpice at this operating point. The waveforms of the resonant capacitor voltage, v_C in Fig 13(a) and inductor current in Fig 13(b), i_L are as predicted in Fig 3. The rectifier input voltage, v_{AB} in also shown in Fig 13(b) indicating the output voltage level of $400V$. Table IV provides a comparison between the predicted values as per the derived closed form expressions and the values seen in the simulation. It can be seen from this table that there's a good correlation between the analysis and simulation results.

TABLE IV: Comparison of analytical and simulation results

Quantity	Analytical	Simulation
Output Voltage, V	400.0V	400.6V
$v_C(0) = m(0) * V_b$	-114.8V	-113.2V
$i_L(0) = j(0) * I_b$	-44.69A	-45.20A
$v_C(\alpha) = m(\alpha) * V_b$	111.2V	111.3V

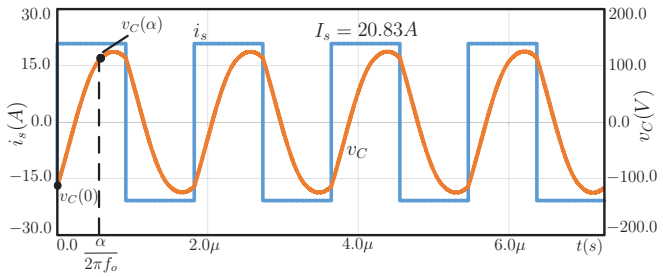

(a)

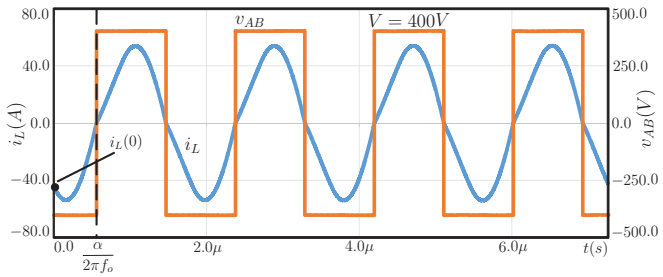

(b)

Fig. 13: Simulation of the current-fed resonant DC/ DC converter at the rated operating point (a) Waveform of the input switching current, i_s and resonant capacitor voltage v_C (b) Waveforms of the resonant inductor current, i_L and secondary AC voltage v_{AB}

Simulation of the converter under the DCM mode of operation was also carried out to validate the converter behaviour. Fig 14 shows i_L and v_{AB} under this condition. The linear rise of the rectifier input voltage when the inductor current is zero validates the DCM mode as predicted in Fig 12.

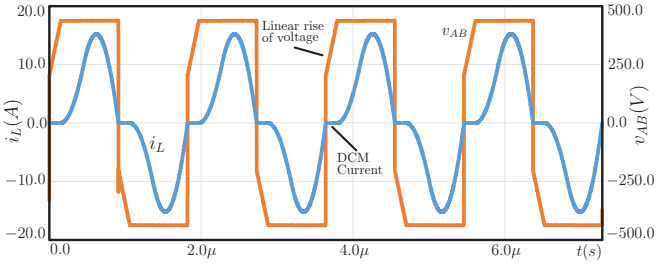

Fig. 14: Simulation of converter under DCM operation. i_L and secondary AC voltage v_{AB} indicating DCM.

IV. Conclusion

This paper introduces a current-fed isolated DC/ DC converter topology with a novel resonant tank circuit for high voltage applications including renewable energy integration. The proposed resonant based modulation and exact analysis of the different operating modes is described in detail. Closed form expressions for the converter gain is derived. The presence of a discontinuous conduction mode and the mode boundary in the output characteristics is discussed. Simulation results validate the operation and presented analysis.

References

[1] C. Iannello, S. Luo, and I. Batarseh, "A full bridge zcs pwm converter for high voltage and high power applications," in *2000 IEEE 31st Annual Power Electronics Specialists Conference. Conference Proceedings (Cat. No.00CH37018)*, vol. 2, 2000, pp. 1064–1071 vol.2.

[2] R. Y. Chen, T. J. Liang, J. F. Chen, R. L. Lin, and K. C. Tseng, "Study and implementation of a current-fed full-bridge boost dc dc converter with zero-current switching for high-voltage applications," *IEEE Transactions on Industry Applications*, vol. 44, no. 4, pp. 1218–1226, July 2008.

[3] P. Xuewei, A. K. Rathore, and U. R. Prasanna, "Novel soft-switching snubberless naturally clamped current-fed full-bridge front-end-converter-based bidirectional inverter for renewables, microgrid, and ups applications," *IEEE Transactions on Industry Applications*, vol. 50, no. 6, pp. 4132–4141, Nov 2014.

[4] A. K. Rathore, D. R. Patil, and D. Srinivasan, "Non-isolated bidirectional soft-switching current-fed lcl resonant dc/dc converter to interface energy storage in dc microgrid," *IEEE Transactions on Industry Applications*, vol. 52, no. 2, pp. 1711–1722, March 2016.

[5] M. Mohr and F. W. Fuchs, "Voltage fed and current fed full bridge converter for the use in three phase grid connected fuel cell systems," in *2006 CES/IEEE 5th International Power Electronics and Motion Control Conference*, vol. 1, Aug 2006, pp. 1–7.

[6] C. Li, Y. Zhang, Z. Cao, and D. XU, "Single-phase single-stage isolated zcs current-fed full-bridge converter for high-power ac/dc applications," *IEEE Transactions on Power Electronics*, vol. 32, no. 9, pp. 6800–6812, Sept 2017.

[7] Y. Shi, R. Li, Y. Xue, and H. Li, "Optimized operation of current-fed dual active bridge dc dc converter for pv applications," *IEEE Transactions on Industrial Electronics*, vol. 62, no. 11, pp. 6986–6995, Nov 2015.

[8] S. Jalbrzykowski and T. Citko, "Current-fed resonant full-bridge boost dc/ac/dc converter," *IEEE Transactions on Industrial Electronics*, vol. 55, no. 3, pp. 1198–1205, March 2008.

[9] S. D. Johnson and R. W. Erickson, "Steady-state analysis and design of the parallel resonant converter," *IEEE Transactions on Power Electronics*, vol. 3, no. 1, pp. 93–104, Jan 1988.